

Search for the chiral magnetic effect via charge-dependent azimuthal correlations relative to spectator and participant planes in Au+Au collisions at $\sqrt{s_{NN}} = 200$ GeV

M. S. Abdallah,⁵ J. Adam,⁶ L. Adamczyk,² J. R. Adams,³⁹ J. K. Adkins,³⁰ G. Agakishiev,²⁸ I. Aggarwal,⁴¹ M. M. Aggarwal,⁴¹ Z. Ahammed,⁶⁰ I. Alekseev,^{3,35} D. M. Anderson,⁵⁵ A. Aparin,²⁸ E. C. Aschenauer,⁶ M. U. Ashraf,¹¹ F. G. Atetalla,²⁹ A. Attri,⁴¹ G. S. Averichev,²⁸ V. Bairathi,⁵³ W. Baker,¹⁰ J. G. Ball Cap,²⁰ K. Barish,¹⁰ A. Behera,⁵² R. Bellwied,²⁰ P. Bhagat,²⁷ A. Bhasin,²⁷ J. Bielcik,¹⁴ J. Bielcikova,³⁸ I. G. Bordyuzhin,³ J. D. Brandenburg,⁶ A. V. Brandin,³⁵ I. Bunzarov,²⁸ J. Butterworth,⁴⁵ X. Z. Cai,⁵⁰ H. Caines,⁶³ M. Calderón de la Barca Sánchez,⁸ D. Cebra,⁸ I. Chakaberia,^{31,6} P. Chaloupka,¹⁴ B. K. Chan,⁹ F.-H. Chang,³⁷ Z. Chang,⁶ N. Chankova-Bunzarova,²⁸ A. Chatterjee,¹¹ S. Chattopadhyay,⁶⁰ D. Chen,¹⁰ J. Chen,⁴⁹ J. H. Chen,¹⁸ X. Chen,⁴⁸ Z. Chen,⁴⁹ J. Cheng,⁵⁷ M. Chevalier,¹⁰ S. Choudhury,¹⁸ W. Christie,⁶ X. Chu,⁶ H. J. Crawford,⁷ M. Csanád,¹⁶ M. Daugherty,¹ T. G. Dedovich,²⁸ I. M. Deppner,¹⁹ A. A. Derevschikov,⁴³ A. Dhamija,⁴¹ L. Di Carlo,⁶² L. Didenko,⁶ X. Dong,³¹ J. L. Drachenberg,¹ J. C. Dunlop,⁶ N. Elsey,⁶² J. Engelage,⁷ G. Eppley,⁴⁵ S. Esumi,⁵⁸ A. Ewigleben,³² O. Eyster,⁶ R. Fatemi,³⁰ F. M. Fawzi,⁵ S. Fazio,⁶ P. Federic,³⁸ J. Fedorisin,²⁸ C. J. Feng,³⁷ Y. Feng,⁴⁴ P. Filip,²⁸ E. Finch,⁵¹ Y. Fisyak,⁶ A. Francisco,⁶³ C. Fu,¹¹ L. Fulek,² C. A. Gagliardi,⁵⁵ T. Galatyuk,¹⁵ F. Geurts,⁴⁵ N. Ghimire,⁵⁴ A. Gibson,⁵⁹ K. Gopal,²³ X. Gou,⁴⁹ D. Grosnick,⁵⁹ A. Gupta,²⁷ W. Gurny,⁶ A. I. Hamad,²⁹ A. Hamed,⁵ Y. Han,⁴⁵ S. Harabasz,¹⁵ M. D. Harasty,⁸ J. W. Harris,⁶³ H. Harrison,³⁰ S. He,¹¹ W. He,¹⁸ X. H. He,²⁶ Y. He,⁴⁹ S. Heppelmann,⁸ S. Heppelmann,⁴² N. Herrmann,¹⁹ E. Hoffman,²⁰ L. Holub,¹⁴ Y. Hu,¹⁸ H. Huang,³⁷ H. Z. Huang,⁹ S. L. Huang,⁵² T. Huang,³⁷ X. Huang,⁵⁷ Y. Huang,⁵⁷ T. J. Humanic,³⁹ G. Igo,^{9,*} D. Isenhower,¹ W. W. Jacobs,²⁵ C. Jena,²³ A. Jentsch,⁶ Y. Ji,³¹ J. Jia,^{6,52} K. Jiang,⁴⁸ X. Ju,⁴⁸ E. G. Judd,⁷ S. Kabana,⁵³ M. L. Kabir,¹⁰ S. Kagamaster,³² D. Kalinkin,^{25,6} K. Kang,⁵⁷ D. Kapukchyan,¹⁰ K. Kauder,⁶ H. W. Ke,⁶ D. Keane,²⁹ A. Kechechyan,²⁸ Y. V. Khyzhniak,³⁵ D. P. Kikoła,⁶¹ C. Kim,¹⁰ B. Kimelman,⁸ D. Kincses,¹⁶ I. Kisel,¹⁷ A. Kiselev,⁶ A. G. Knospe,³² L. Kochenda,³⁵ L. K. Kosarzewski,¹⁴ L. Kramarik,¹⁴ P. Kravtsov,³⁵ L. Kumar,⁴¹ S. Kumar,²⁶ R. Kunnawalkam Elayavalli,⁶³ J. H. Kwasizur,²⁵ S. Lan,¹¹ J. M. Landgraf,⁶ J. Lauret,⁶ A. Lebedev,⁶ R. Lednicky,²⁸ J. H. Lee,⁶ Y. H. Leung,³¹ C. Li,⁴⁹ C. Li,⁴⁸ W. Li,⁴⁵ X. Li,⁴⁸ Y. Li,⁵⁷ X. Liang,¹⁰ Y. Liang,²⁹ R. Licenik,³⁸ T. Lin,⁵⁵ Y. Lin,¹¹ M. A. Lisa,³⁹ F. Liu,¹¹ H. Liu,²⁵ H. Liu,¹¹ P. Liu,⁵² T. Liu,⁶³ X. Liu,³⁹ Y. Liu,⁵⁵ Z. Liu,⁴⁸ T. Ljubicic,⁶ W. J. Llope,⁶² R. S. Longacre,⁶ E. Loyd,¹⁰ N. S. Lukow,⁵⁴ X. Luo,¹¹ L. Ma,¹⁸ R. Ma,⁶ Y. G. Ma,¹⁸ N. Magdy,¹² R. Majka,^{63,*} D. Mallick,³⁶ S. Margetis,²⁹ C. Markert,⁵⁶ H. S. Matis,³¹ J. A. Mazer,⁴⁶ N. G. Minaev,⁴³ S. Mioduszewski,⁵⁵ B. Mohanty,³⁶ M. M. Mondal,⁵² I. Mooney,⁶² D. A. Morozov,⁴³ A. Mukherjee,¹⁶ M. Nagy,¹⁶ J. D. Nam,⁵⁴ Md. Nasim,²² K. Nayak,¹¹ D. Neff,⁹ J. M. Nelson,⁷ D. B. Nemes,⁶³ M. Nie,⁴⁹ G. Nigmatkulov,³⁵ T. Niida,⁵⁸ R. Nishitani,⁵⁸ L. V. Nogach,⁴³ T. Nonaka,⁵⁸ A. S. Nunes,⁶ G. Odyniec,³¹ A. Ogawa,⁶ S. Oh,³¹ V. A. Okorokov,³⁵ B. S. Page,⁶ R. Pak,⁶ A. Pandav,³⁶ A. K. Pandey,⁵⁸ Y. Panebratsev,²⁸ P. Parfenov,³⁵ B. Pawlik,⁴⁰ D. Pawlowska,⁶¹ H. Pei,¹¹ C. Perkins,⁷ L. Pinsky,²⁰ R. L. Pintér,¹⁶ J. Pluta,⁶¹ B. R. Pokhrel,⁵⁴ G. Pomatkin,³⁸ J. Porter,³¹ M. Posik,⁵⁴ V. Prozorova,¹⁴ N. K. Pruthi,⁴¹ M. Przybycien,² J. Putschke,⁶² H. Qiu,²⁶ A. Quintero,⁵⁴ C. Racz,¹⁰ S. K. Radhakrishnan,²⁹ N. Raha,⁶² R. L. Ray,⁵⁶ R. Reed,³² H. G. Ritter,³¹ M. Robotkova,³⁸ O. V. Rogachevskiy,²⁸ J. L. Romero,⁸ L. Ruan,⁶ J. Rusnak,³⁸ N. R. Sahoo,⁴⁹ H. Sako,⁵⁸ S. Salur,⁴⁶ J. Sandweiss,^{63,*} S. Sato,⁵⁸ W. B. Schmidke,⁶ N. Schmitz,³³ B. R. Schweid,⁵² F. Seck,¹⁵ J. Seger,¹³ M. Sergeeva,⁹ R. Seto,¹⁰ P. Seyboth,³³ N. Shah,²⁴ E. Shahaliev,²⁸ P. V. Shanmuganathan,⁶ M. Shao,⁴⁸ T. Shao,⁵⁰ A. I. Sheikh,²⁹ D. Shen,⁵⁰ S. S. Shi,¹¹ Y. Shi,⁴⁹ Q. Y. Shou,¹⁸ E. P. Sichtermann,³¹ R. Sikora,² M. Simko,³⁸ J. Singh,⁴¹ S. Singha,²⁶ M. J. Skoby,⁴⁴ N. Smirnov,⁶³ Y. Söhnngen,¹⁹ W. Solyst,²⁵ P. Sorensen,⁶ H. M. Spinka,^{4,*} B. Srivastava,⁴⁴ T. D. S. Stanislaus,⁵⁹ M. Stefaniak,⁶¹ D. J. Stewart,⁶³ M. Strikhanov,³⁵ B. Stringfellow,⁴⁴ A. A. P. Suaide,⁴⁷ M. Sumner,³⁸ B. Summa,⁴² X. M. Sun,¹¹ X. Sun,¹² Y. Sun,⁴⁸ Y. Sun,²¹ B. Surov,⁵⁴ D. N. Svirida,³ Z. W. Sweger,⁸ P. Szymanski,⁶¹ A. H. Tang,⁶ Z. Tang,⁴⁸ A. Taranenko,³⁵ T. Tarnowsky,³⁴ J. H. Thomas,³¹ A. R. Timmins,²⁰ D. Tlusty,¹³ T. Todoroki,⁵⁸ M. Tokarev,²⁸ C. A. Tomkiel,³² S. Trentalange,⁹ R. E. Tribble,⁵⁵ P. Tribedy,⁶ S. K. Tripathy,¹⁶ T. Truhlar,¹⁴ B. A. Trzeciak,¹⁴ O. D. Tsai,⁹ Z. Tu,⁶ T. Ullrich,⁶ D. G. Underwood,⁴ I. Upsal,^{49,6} G. Van Buren,⁶ J. Vanek,³⁸ A. N. Vasiliev,⁴³ I. Vassiliev,¹⁷ V. Verkest,⁶² F. Videbæk,⁶ S. Vokal,²⁸ S. A. Voloshin,⁶² F. Wang,⁴⁴ G. Wang,⁹ J. S. Wang,²¹ P. Wang,⁴⁸ Y. Wang,¹¹ Y. Wang,⁵⁷ Z. Wang,⁴⁹ J. C. Webb,⁶ P. C. Weidenkaff,¹⁹ L. Wen,⁹ G. D. Westfall,³⁴ H. Wieman,³¹ S. W. Wissink,²⁵ J. Wu,²⁶ Y. Wu,¹⁰ B. Xi,⁵⁰ Z. G. Xiao,⁵⁷ G. Xie,³¹ W. Xie,⁴⁴ H. Xu,²¹ N. Xu,³¹ Q. H. Xu,⁴⁹ Y. Xu,⁴⁹ Z. Xu,⁶ Z. Xu,⁹ C. Yang,⁴⁹ Q. Yang,⁴⁹ S. Yang,⁴⁵ Y. Yang,³⁷ Z. Ye,⁴⁵ Z. Ye,¹² L. Yi,⁴⁹ K. Yip,⁶ Y. Yu,⁴⁹ H. Zbroszczyk,⁶¹ W. Zha,⁴⁸ C. Zhang,⁵² D. Zhang,¹¹ S. Zhang,¹² S. Zhang,¹⁸ X. P. Zhang,⁵⁷ Y. Zhang,²⁶ Y. Zhang,⁴⁸ Y. Zhang,¹¹

Z. J. Zhang,³⁷ Z. Zhang,⁶ Z. Zhang,¹² J. Zhao,⁴⁴ C. Zhou,¹⁸ X. Zhu,⁵⁷ Z. Zhu,⁴⁹ M. Zurek,³¹ and M. Zyzak¹⁷
(STAR Collaboration)

- ¹Abilene Christian University, Abilene, Texas 79699
²AGH University of Science and Technology, FPACS, Cracow 30-059, Poland
³Alikhanov Institute for Theoretical and Experimental Physics NRC "Kurchatov Institute", Moscow 117218, Russia
⁴Argonne National Laboratory, Argonne, Illinois 60439
⁵American University of Cairo, New Cairo 11835, New Cairo, Egypt
⁶Brookhaven National Laboratory, Upton, New York 11973
⁷University of California, Berkeley, California 94720
⁸University of California, Davis, California 95616
⁹University of California, Los Angeles, California 90095
¹⁰University of California, Riverside, California 92521
¹¹Central China Normal University, Wuhan, Hubei 430079
¹²University of Illinois at Chicago, Chicago, Illinois 60607
¹³Creighton University, Omaha, Nebraska 68178
¹⁴Czech Technical University in Prague, FNSPE, Prague 115 19, Czech Republic
¹⁵Technische Universität Darmstadt, Darmstadt 64289, Germany
¹⁶ELTE Eötvös Loránd University, Budapest, Hungary H-1117
¹⁷Frankfurt Institute for Advanced Studies FIAS, Frankfurt 60438, Germany
¹⁸Fudan University, Shanghai, 200433
¹⁹University of Heidelberg, Heidelberg 69120, Germany
²⁰University of Houston, Houston, Texas 77204
²¹Huzhou University, Huzhou, Zhejiang 313000
²²Indian Institute of Science Education and Research (IISER), Berhampur 760010, India
²³Indian Institute of Science Education and Research (IISER) Tirupati, Tirupati 517507, India
²⁴Indian Institute Technology, Patna, Bihar 801106, India
²⁵Indiana University, Bloomington, Indiana 47408
²⁶Institute of Modern Physics, Chinese Academy of Sciences, Lanzhou, Gansu 730000
²⁷University of Jammu, Jammu 180001, India
²⁸Joint Institute for Nuclear Research, Dubna 141 980, Russia
²⁹Kent State University, Kent, Ohio 44242
³⁰University of Kentucky, Lexington, Kentucky 40506-0055
³¹Lawrence Berkeley National Laboratory, Berkeley, California 94720
³²Lehigh University, Bethlehem, Pennsylvania 18015
³³Max-Planck-Institut für Physik, Munich 80805, Germany
³⁴Michigan State University, East Lansing, Michigan 48824
³⁵National Research Nuclear University MEPHI, Moscow 115409, Russia
³⁶National Institute of Science Education and Research, HBNI, Jatni 752050, India
³⁷National Cheng Kung University, Tainan 70101
³⁸Nuclear Physics Institute of the CAS, Rez 250 68, Czech Republic
³⁹Ohio State University, Columbus, Ohio 43210
⁴⁰Institute of Nuclear Physics PAN, Cracow 31-342, Poland
⁴¹Panjab University, Chandigarh 160014, India
⁴²Pennsylvania State University, University Park, Pennsylvania 16802
⁴³NRC "Kurchatov Institute", Institute of High Energy Physics, Protvino 142281, Russia
⁴⁴Purdue University, West Lafayette, Indiana 47907
⁴⁵Rice University, Houston, Texas 77251
⁴⁶Rutgers University, Piscataway, New Jersey 08854
⁴⁷Universidade de São Paulo, São Paulo, Brazil 05314-970
⁴⁸University of Science and Technology of China, Hefei, Anhui 230026
⁴⁹Shandong University, Qingdao, Shandong 266237
⁵⁰Shanghai Institute of Applied Physics, Chinese Academy of Sciences, Shanghai 201800
⁵¹Southern Connecticut State University, New Haven, Connecticut 06515
⁵²State University of New York, Stony Brook, New York 11794
⁵³Instituto de Alta Investigación, Universidad de Tarapacá, Arica 1000000, Chile
⁵⁴Temple University, Philadelphia, Pennsylvania 19122
⁵⁵Texas A&M University, College Station, Texas 77843
⁵⁶University of Texas, Austin, Texas 78712
⁵⁷Tsinghua University, Beijing 100084
⁵⁸University of Tsukuba, Tsukuba, Ibaraki 305-8571, Japan
⁵⁹Valparaiso University, Valparaiso, Indiana 46383
⁶⁰Variable Energy Cyclotron Centre, Kolkata 700064, India
⁶¹Warsaw University of Technology, Warsaw 00-661, Poland

⁶²Wayne State University, Detroit, Michigan 48201

⁶³Yale University, New Haven, Connecticut 06520

(Dated: June 18, 2021)

The chiral magnetic effect (CME) refers to charge separation along a strong magnetic field due to imbalanced chirality of quarks in local parity and charge-parity violating domains in quantum chromodynamics. The experimental measurement of the charge separation is made difficult by the presence of a major background from elliptic azimuthal anisotropy. This background and the CME signal have different sensitivities to the spectator and participant planes, and could thus be determined by measurements with respect to these planes. We report such measurements in Au+Au collisions at a nucleon-nucleon center-of-mass energy of 200 GeV at the Relativistic Heavy-Ion Collider. It is found that the charge separation, with the flow background removed, is consistent with zero in peripheral (large impact parameter) collisions. Some indication of finite CME signals is seen with a significance of 1–3 standard deviations in mid-central (intermediate impact parameter) collisions. Significant residual background effects may, however, still be present.

PACS numbers: 25.75.-q, 25.75.Gz, 25.75.Ld

Introduction. Metastable domains of fluctuating topological charges can change the chirality of quarks and induce local parity and charge-parity violation in quantum chromodynamics (QCD) [1–3]. This would lead to an electric charge separation in the presence of a strong magnetic field, a phenomenon known as the chiral magnetic effect (CME) [2–5]. Such a magnetic field, as strong as 10^{18} G, may be present in non-central (nonzero impact parameter) relativistic heavy-ion collisions, generated by the spectator protons (i.e., those that do not participate in the collision) at early times [4–7]. While a finite CME signal is generally expected in those collisions [3, 4], quantitative predictions beyond order-of-magnitude estimates are not yet at hand [8] despite extensive theoretical developments over the last decade (see recent reviews [9–12]). Meanwhile, experimental efforts have been devoted to searching for the CME-induced charge separation at the Relativistic Heavy-Ion Collider (RHIC) and the Large Hadron Collider (LHC) (see reviews in Refs. [10, 13–16]), including a dedicated run of isobar collisions at RHIC [17, 18].

The magnetic field direction in heavy-ion collisions is perpendicular to the spectator proton plane (defined by the beam direction and the average transverse position of spectator protons). It coincides approximately with the spectator neutron plane, or simply the spectator plane (SP) [19]. The participant plane (PP, defined by the beam direction and the average transverse position of the participant nucleons) does not coincide with the SP because of large event-by-event fluctuations of the PP [20, 21]. These fluctuations are the single most important factor that motivates the methodology [19, 22] for the measurements reported in this paper. Experimentally, the SP can be accessed by detecting forward-emitted neutrons, and the PP can be approximated by the direction of maximum final-state particle azimuthal density.

The commonly used observable to measure the charge separation is the three-point correlator [23], $\gamma\{\psi\} \equiv \cos(\phi_\alpha + \phi_\beta - 2\psi)$, where ϕ_α and ϕ_β are the azimuthal

angles of particles α and β , respectively, and ψ is the azimuthal angle of either the SP (ψ_{SP}) or the PP (ψ_{PP}). Because of the charge-independent correlation backgrounds (e.g. from global momentum conservation), often the correlator difference is used, $\Delta\gamma\{\psi\} \equiv \gamma_{\text{OS}}\{\psi\} - \gamma_{\text{SS}}\{\psi\}$, where “OS” (“SS”) refers to the opposite-sign (same-sign) electric charges of particles α and β . A CME signal, often characterized by the Fourier coefficient a_1 in the final-state azimuthal distributions of positive (+) and negative (−) hadrons, $\frac{dN_\pm}{d\phi_\pm} \propto 1 \pm 2a_1 \sin(\phi_\pm - \psi) + 2v_2 \cos 2(\phi_\pm - \psi) + \dots$, would yield a magnitude of $\Delta\gamma = 2a_1^2$ [23]. The v_2 is the elliptic flow anisotropy arising from strong (partonic) interactions converting the initial geometric anisotropy of the participant nucleons into momentum-space anisotropy of final-state hadrons [24].

Significant $\Delta\gamma\{\psi_{\text{PP}}\}$ and $\Delta\gamma\{\psi_{\text{SP}}\}$, on the order of 10^{-4} , have indeed been observed in relativistic heavy-ion collisions [25–29]. The interpretation of $\Delta\gamma$ originating from CME-induced charge separation is difficult due to the presence of charge-dependent backgrounds, such as those from resonance decays [23, 30–34] via

$$\Delta\gamma_{\text{bkgd}} \propto \langle \cos(\phi_\alpha + \phi_\beta - 2\phi_{\text{res}}) \rangle v_{2,\text{res}}, \quad (1)$$

where $v_{2,\text{res}} = \langle \cos 2(\phi_{\text{res}} - \psi) \rangle$ is the resonance v_2 relative to ψ [35]. Moreover, comparable $\Delta\gamma\{\psi_{\text{PP}}\}$ has also been observed in small system collisions [36–38], where any CME-induced charge separation is expected to be randomly oriented relative to the ψ_{PP} [36, 39] and thus unobservable in experiments. Because of those major backgrounds no firm conclusion can so far be drawn regarding the existence of the CME in relativistic heavy-ion collisions. Various approaches have been applied to deal with the background [37, 40–42]. In this paper, we present a search for the CME with a new approach first proposed in Ref. [19] and followed by Ref. [43].

Methodology. The hypothesized CME-driven charge separation is along the magnetic field, mainly from spectator protons, and is therefore the strongest in the di-

rection perpendicular to ψ_{SP} . The major background to the CME is related to v_2 , determined by the participant geometry, and is therefore the largest along ψ_{PP} . The $\Delta\gamma\{\psi_{\text{SP}}\}$ and $\Delta\gamma\{\psi_{\text{PP}}\}$ measured relative to ψ_{SP} and ψ_{PP} , therefore, contain different amounts of the CME and background, and this offers the opportunity to determine these two contributions uniquely [19]. Consider the measured $\Delta\gamma$ to be composed of the v_2 background ($\Delta\gamma_{\text{bkgd}}$) and the CME signal ($\Delta\gamma_{\text{CME}}$). Assuming $\Delta\gamma_{\text{bkgd}}$ is proportional to v_2 (Eq. (1)) and the $\Delta\gamma_{\text{CME}}$ -inducing magnetic field is determined by spectators, both “projected” onto the ψ direction, we have $\Delta\gamma_{\text{CME}}\{\psi_{\text{PP}}\} = a\Delta\gamma_{\text{CME}}\{\psi_{\text{SP}}\}$ and $\Delta\gamma_{\text{bkgd}}\{\psi_{\text{SP}}\} = a\Delta\gamma_{\text{bkgd}}\{\psi_{\text{PP}}\}$ [19]. Here the projection factor $a = \langle \cos 2(\psi_{\text{PP}} - \psi_{\text{SP}}) \rangle$ comes directly out of the definitions of the v_2 and $\Delta\gamma$ variables, and can be readily obtained from the v_2 measurements:

$$a = v_2\{\psi_{\text{SP}}\}/v_2\{\psi_{\text{PP}}\}. \quad (2)$$

It does not assume any particular physics, such as the event-plane decorrelation over rapidity [44–46]. The CME signal relative to the inclusive $\Delta\gamma\{\psi_{\text{PP}}\}$ measurement is then given by [19]

$$f_{\text{CME}} = \frac{\Delta\gamma_{\text{CME}}\{\psi_{\text{PP}}\}}{\Delta\gamma\{\psi_{\text{PP}}\}} = \frac{A/a - 1}{1/a^2 - 1}, \quad (3)$$

where

$$A = \Delta\gamma\{\psi_{\text{SP}}\}/\Delta\gamma\{\psi_{\text{PP}}\}. \quad (4)$$

The above formalism applies even when the magnetic field direction does not coincide with ψ_{SP} as long as its fluctuations are independent from those of the ψ_{PP} [19]. It is possible, however, that the magnetic field projection factor is not strictly a because of final-state evolution effects on the charge separation [47]. If instead $\Delta\gamma_{\text{CME}}\{\psi_{\text{PP}}\} = b\Delta\gamma_{\text{CME}}\{\psi_{\text{SP}}\}$, then Eq. (3) becomes $f_{\text{CME}} = \frac{A/a-1}{1/(ab)-1}$, a factor of $\frac{b/a-ab}{1-ab}$ different. A full study of this would require rigorous theoretical input and is beyond the scope of the present work. In this paper we report the measured v_2 and $\Delta\gamma$ with respect to ψ_{SP} and ψ_{PP} , and use Eq. (3) to extract the possible CME signal.

Data Analysis. The data reported here are from Au+Au collisions taken by the STAR experiment at a nucleon-nucleon center-of-mass energy of $\sqrt{s_{\text{NN}}} = 200$ GeV in the years 2011, 2014 and 2016. A minimum-bias (MB) trigger was provided by a coincidence signal between the vertex position detectors located at forward/backward pseudo-rapidities (η) $4.24 < |\eta| < 5.1$. Two zero-degree hadron calorimeters (ZDCs) [48] are located at ± 18 m along the beam (z) direction from the nominal interaction point at the center of the STAR detector. Each has an approximate 5 mrad aperture and

intercepts fragmented spectator neutrons from the colliding beams. Within the ZDCs, shower maximum detectors (SMD) were installed to measure the spatial distributions of those spectator neutrons [49].

The details of the STAR experimental apparatus are described elsewhere [50]. The main tracking detector of the STAR experiment is the cylindrical Time Projection Chamber (TPC) [51, 52]. The TPC provides full azimuthal coverage ($0 < \phi < 2\pi$) and a coverage in η of $-1.2 < \eta < 1.2$. Track trajectories are reconstructed from 3-dimensional hit points recorded by the TPC; at least 10 out of a possible maximum of 45 points are required for a valid track. The TPC resides in a uniform 0.5 Tesla magnetic field along the $-z$ direction, allowing determination of particle momenta from the track curvature for transverse momenta $p_{\text{T}} > 0.15$ GeV/ c . The primary vertex of a collision is reconstructed from charged particle tracks. Events with primary vertices within 30 cm (year 2011) or 6 cm (years 2014 and 2016, taken with the heavy flavor tracker [53]) longitudinally and 2 cm transversely from the geometrical center of the TPC are used, providing a total of 2.4 billion MB events. Collision centrality is determined from the multiplicity of charged particles within a distance of closest approach (DCA) to the primary vertex of less than 3 cm and within an η range of $|\eta| < 0.5$ [54].

Tracks used for the correlation analysis reported in this paper are required to have stricter criteria: at least 20 points used in track fitting, and DCA less than 1 cm. The fraction of fit points used to determine a track relative to the maximum number of points possible for that track given the TPC geometry, is required to be greater than 0.52 to avoid double counting of split tracks.

Experimentally, the ψ_{SP} can be assessed by the first order harmonic plane of spectator neutrons measured by the ZDC-SMD, and the ψ_{PP} can be assessed by the second order harmonic event plane of mid-rapidity tracks measured by the TPC [35]. In the rest of the paper, we refer to the former as ψ_{ZDC} and the latter as ψ_{TPC} . In this analysis, the γ and v_2 are calculated by $\gamma = \langle \cos(\phi_{\alpha} + \phi_{\beta} - 2\psi_{\text{rec}}) \rangle / R$ and $v_2 = \langle \cos 2(\phi_{\alpha, \beta} - \psi_{\text{rec}}) \rangle / R$, where ψ_{rec} is either ψ_{ZDC} or ψ_{TPC} , and R is the corresponding resolution [35]. The same particles of interest (POI), denoted by α and β , are used for γ and v_2 with p_{T} from 0.2 to 2 GeV/ c . Two methods are employed in this analysis. The first one, referred to as the “full-event” method, uses particles from $|\eta| < 1$ as the POI. A third particle (c) from the same acceptance is used in place of ψ_{TPC} , and R equals the particle $v_{2,c}$ [25]. For this method, another p_{T} range from 0.2 to 1 GeV/ c is also analyzed for POI to explore possible p_{T} dependence of the CME signal, speculated to be dominant at low p_{T} [4]. The second method, referred to as the “sub-event” method, divides the TPC particles into two sub-events symmetric about mid-rapidity [35], where α and β are from one sub-event, and the ψ_{TPC} is recon-

structed from the other. This procedure suppresses non-flow correlations that are short-ranged, such as those due to resonance decays and jets [30, 55, 56], by applying an η gap ($\Delta\eta_{\text{sub}}$) between the two subevents. We perform the analyses with $\Delta\eta_{\text{sub}} = 0.1$ and $\Delta\eta_{\text{sub}} = 0.3$ (e.g. for the former, with one sub-event from $\eta > 0.05$ and the other from $\eta < -0.05$). The R is calculated from the correlations between the two TPC sub-events [35]. For measurements relative to the ψ_{ZDC} , the POI (α and β) are still from the same TPC acceptance corresponding to the full-event or sub-event method. An event-plane vector is determined in each ZDC from its measured energy distribution. The two event-plane vectors are combined to give ψ_{ZDC} and their correlations give R [35, 49].

Systematic Uncertainties. To investigate the effect of track fitting quality, we vary the minimum number of hit points used in track fitting from the default 20 to 15 and 25. To investigate the effect of secondary particle contamination, we vary the maximum DCA of a track from the default 1.0 cm to 3.0, 2.0, and 0.8 cm. With each variation, the full analysis is repeated and results from different years are combined at the end. In quoting the centrality-integrated results, results from different centralities are combined before the result is compared to the default case. In this way, the (anti-)correlations in the uncertainties are properly taken into account. In the systematic uncertainty estimation of each source, the statistical fluctuation effect arising from the change in the data sample due to each variation, is subtracted; when the change in the result is smaller than the statistical fluctuation, the systematic uncertainty is set to zero [57]. For each source when multiple variations are used, the systematic uncertainty is taken as the RMS. In order to minimize fluctuations due to the limited statistics, the systematic uncertainties for the entire 20–80% centrality range as well as for the 20–50% and 50–80% ranges are evaluated. The larger value among the 20–80% centrality range and the 20–50% (or 50–80%) range is quoted, unless both are zero (i.e., results are consistent within statistical fluctuations); in this case, the systematic uncertainties (evaluated from the individual centralities) are presented. For the 20–50% centrality, the resultant absolute systematic uncertainties on $\langle f_{\text{CME}} \rangle$ for $0.2 < p_T < 2.0$ GeV/ c with the full-event method are 2.2% and 1.3% for the number of hits and DCA variations, respectively.

In order to investigate any acceptance effects due to the vertex z position, we separate events into positive and negative vertex z samples. Their differences from the combined sample beyond statistical fluctuations are included in the systematic uncertainties [57]. For the 20–50% centrality range, the results for $\langle f_{\text{CME}} \rangle$ are consistent within statistical uncertainties between positive and negative vertex z events; therefore systematic uncertainties evaluated for individual centralities are presented. For the 50–80% centrality range, the combined systematic uncertainty is used.

The variations in the results among the three run periods (years 2011, 2014 and 2016) beyond statistical fluctuations are taken as part of the systematic uncertainties. For $\langle f_{\text{CME}} \rangle$, the results are consistent within statistical uncertainties.

To investigate the effect of the ZDC harmonic plane determination, analyses are also performed using only a single ZDC side for ψ_{ZDC} as well as an arithmetic average of the ψ_{ZDC} values from the two sides. The results are consistent with the default case within statistical uncertainties.

The ϕ -dependent track reconstruction efficiency is corrected in our analysis. We investigated the effect of applying a p_T -dependent efficiency correction and find no significant deviations in the final results.

The systematic uncertainties from the various sources are added in quadrature and are quoted with one standard deviation.

Results. Figure 1, panels (a) and (b) show, respectively, the measured v_2 and $\Delta\gamma$ with respect to the ψ_{ZDC} and ψ_{TPC} from the full-event method with $0.2 < p_T < 2$ GeV/ c in Au+Au collisions at $\sqrt{s_{\text{NN}}} = 200$ GeV as a function of collision centrality. The $v_2\{\psi_{\text{ZDC}}\}$ is smaller than $v_2\{\psi_{\text{TPC}}\}$, as expected; the ratio of the two gives the quantity a as specified by Eq. (2). The $\Delta\gamma\{\psi_{\text{ZDC}}\}$ is also smaller than $\Delta\gamma\{\psi_{\text{TPC}}\}$, as expected if they are dominated by v_2 backgrounds; the ratio of the two gives the quantity A as specified by Eq. (4). Figure 1(c) shows the quantities a and A as functions of centrality. The values of A and a are found to be nearly identical over the full centrality range, indicating the dominance of background contributions in $\Delta\gamma\{\psi_{\text{TPC}}\}$ and $\Delta\gamma\{\psi_{\text{ZDC}}\}$.

Figure 2(a) shows the A/a ratio from both the full-event and sub-event methods, both for $0.2 < p_T < 2$ GeV/ c . A value of $A/a > 1$ would indicate the possible existence of a CME signal. Figure 2(b) shows the centrality dependence of f_{CME} , the possible CME signal relative to the inclusive measurement $\Delta\gamma\{\psi_{\text{TPC}}\}$, extracted by Eq. (3). Figure 2(c) shows the absolute magnitude of the signal, $\Delta\gamma_{\text{CME}} = f_{\text{CME}}\Delta\gamma_{\text{inc}}$ (here $\Delta\gamma_{\text{CME}} \equiv \Delta\gamma_{\text{CME}}\{\psi_{\text{TPC}}\}$ and $\Delta\gamma_{\text{inc}} \equiv \Delta\gamma\{\psi_{\text{TPC}}\}$), as a function of centrality. The statistical uncertainty is propagated from the four measured quantities $\Delta\gamma\{\psi_{\text{ZDC}}\}$, $\Delta\gamma\{\psi_{\text{TPC}}\}$, $v_2\{\psi_{\text{ZDC}}\}$, and $v_2\{\psi_{\text{TPC}}\}$, not from f_{CME} and $\Delta\gamma_{\text{inc}}$ in the product.

Table I reports $\langle f_{\text{CME}} \rangle$ and $\langle \Delta\gamma_{\text{CME}} \rangle$, averaged over 20–50% and 50–80% centrality ranges, along with the inclusive $\langle \Delta\gamma_{\text{inc}} \rangle$. Both the full-event and sub-event methods are tabulated. In addition to the p_T range $0.2 < p_T < 2$ GeV/ c , a lower p_T range $0.2 < p_T < 1$ GeV/ c for the POI is also listed for the full-event method. Two η gaps are quoted for the sub-event results. The systematic uncertainty on $\langle \Delta\gamma_{\text{CME}} \rangle$ is larger than that on $\langle f_{\text{CME}} \rangle$, because some of the systematics are canceled in f_{CME} but not in $\Delta\gamma_{\text{CME}}$.

Figure 3 depicts the possible CME signal $\langle f_{\text{CME}} \rangle$ and

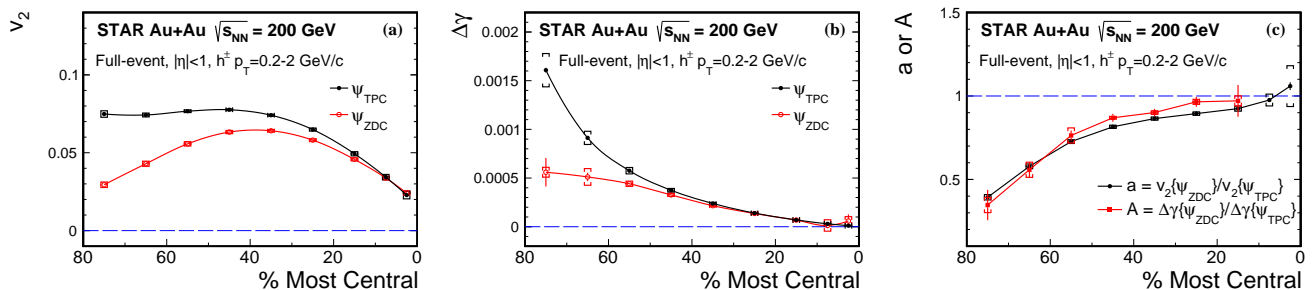


FIG. 1. The centrality dependencies of the v_2 (a) and $\Delta\gamma$ (b) measured with respect to ψ_{ZDC} and ψ_{TPC} from the full-event method. Panel (c) presents the ratios a and A . Error bars show statistical uncertainties; the caps indicate the systematic uncertainties.

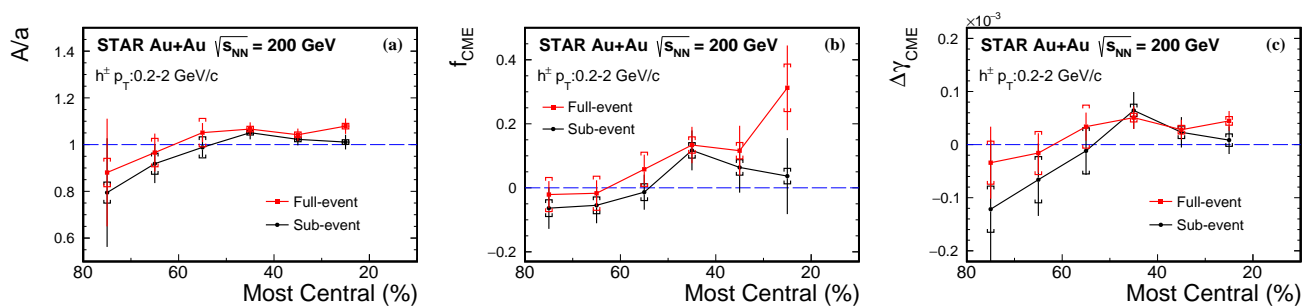


FIG. 2. The A/a ratio (a), the extracted f_{CME} (b), and $\Delta\gamma_{\text{CME}}$ (c) as functions of the collision centrality from the full-event and sub-event ($\Delta\eta_{\text{sub}} = 0.1$) methods. Error bars show statistical uncertainties; the caps indicate the systematic uncertainties.

$\langle\Delta\gamma_{\text{CME}}\rangle$ averaged in 20–50% and 50–80% centralities of Au+Au collisions, extracted from various methods. Signals are consistent with zero in the 50–80% peripheral centrality range. For the 20–50% centrality range, a hint of deviation from zero is seen with 1–3 standard deviations, depending on whether or not an η gap is applied, and on the size of the applied η gap. Note that the statistical and systematic uncertainties among the data points are not completely independent of each other because the same overall data sample is used in the various methods.

Discussion. While some hint of nonzero f_{CME} is suggested, especially from the full-event method, a key assumption is made that the flow background is proportional to the final-state hadron v_2 [19]. However, this assumption does not strictly hold because of the presence of non-flow. For example, two-particle correlations contribute positively to $v_2\{\psi_{\text{TPC}}\}$, which would reduce a , yielding an increased f_{CME} . Three-particle correlations could significantly increase $\Delta\gamma\{\psi_{\text{TPC}}\}$, which would reduce A , and thus cause a decreased f_{CME} . The relative strengths of those effects on f_{CME} are unknown a priori. The measured f_{CME} and $\Delta\gamma_{\text{CME}}$ can, therefore, still be contaminated by non-flow effects. In order to mitigate non-flow effects, we have also analyzed data using the sub-event method with two η gaps. The extracted f_{CME} and $\Delta\gamma_{\text{CME}}$, however, have reduced significance because

of the smaller particle pair statistics with the sub-event method and presumably smaller non-flow contributions. Our result is consistent with the previously extracted $f_{\text{CME}} = (2 \pm 4 \pm 5)\%$ [40] (also from the sub-event method) exploiting the pair invariant mass [58]. The method exploited in the present work uses additional information from the ZDCs and takes advantage of the PP and SP fluctuations.

The CME is speculated to be a low- p_{T} phenomenon [4]. Our previous inclusive $\Delta\gamma_{\text{inc}}$ results [25, 26], as well as those reported here, indicate that the $\Delta\gamma_{\text{inc}}$ increases with p_{T} of the POI. In this work, we have also investigated a lower p_{T} range, $0.2 < p_{\text{T}} < 1$ GeV/c, using the full-event method. Given the large uncertainties we cannot draw conclusions concerning the relative magnitude of f_{CME} or $\Delta\gamma_{\text{CME}}$ between the two p_{T} ranges.

Conclusions. In summary, we have reported measurements of the elliptic flow anisotropy v_2 and three-particle correlator $\Delta\gamma$ with respect to the first-order harmonic plane from the zero-degree calorimeters, ψ_{ZDC} , and the second-order harmonic plane from the time projection chamber, ψ_{TPC} . We used the full-event method where the particles of interest POI and ψ_{TPC} are both from the $|\eta| < 1$ range, and studied two p_{T} ranges for the POI. We also used the sub-event method where the POI and ψ_{TPC} are from two sub-events, and we applied two

TABLE I. The inclusive $\langle \Delta\gamma_{\text{inc}} \rangle \equiv \langle \Delta\gamma\{\psi_{\text{TPC}}\} \rangle$ and the extracted $\langle f_{\text{CME}} \rangle$ and $\langle \Delta\gamma_{\text{CME}} \rangle$, averaged over 20–50% and 50–80% centrality ranges in Au+Au collisions at $\sqrt{s_{\text{NN}}} = 200$ GeV from the full-event method (with two POI p_T ranges) and the sub-event method (with two η gaps). The first quoted uncertainty is statistical and the second systematic.

Centrality	Method	$\langle \Delta\gamma_{\text{inc}} \rangle (\times 10^{-4})$	$\langle f_{\text{CME}} \rangle (\%)$	$\langle \Delta\gamma_{\text{CME}} \rangle (\times 10^{-4})$
20–50%	full-event, $p_T=0.2-2$ GeV/c	$1.89 \pm 0.01 \pm 0.10$	$14.7 \pm 4.3 \pm 2.6$	$0.40 \pm 0.11 \pm 0.08$
	full-event, $p_T=0.2-1$ GeV/c	$1.48 \pm 0.01 \pm 0.07$	$13.7 \pm 6.2 \pm 2.3$	$0.29 \pm 0.13 \pm 0.06$
	sub-event, $\Delta\eta_{\text{sub}}=0.1$, $p_T=0.2-2$ GeV/c	$2.84 \pm 0.01 \pm 0.15$	$8.8 \pm 4.5 \pm 2.4$	$0.27 \pm 0.17 \pm 0.12$
	sub-event, $\Delta\eta_{\text{sub}}=0.3$, $p_T=0.2-2$ GeV/c	$2.94 \pm 0.01 \pm 0.15$	$6.3 \pm 5.0 \pm 2.5$	$0.23 \pm 0.19 \pm 0.14$
50–80%	full-event, $p_T=0.2-2$ GeV/c	$6.31 \pm 0.03 \pm 0.38$	$0.3 \pm 2.5 \pm 5.3$	$0.12 \pm 0.21 \pm 0.40$
	full-event, $p_T=0.2-1$ GeV/c	$5.19 \pm 0.04 \pm 0.33$	$4.6 \pm 3.4 \pm 7.3$	$0.37 \pm 0.23 \pm 0.41$
	sub-event, $\Delta\eta_{\text{sub}}=0.1$, $p_T=0.2-2$ GeV/c	$8.72 \pm 0.06 \pm 0.41$	$-4.2 \pm 3.4 \pm 2.6$	$-0.36 \pm 0.36 \pm 0.43$
	sub-event, $\Delta\eta_{\text{sub}}=0.3$, $p_T=0.2-2$ GeV/c	$8.89 \pm 0.07 \pm 0.40$	$-4.6 \pm 3.9 \pm 2.7$	$-0.46 \pm 0.43 \pm 0.45$

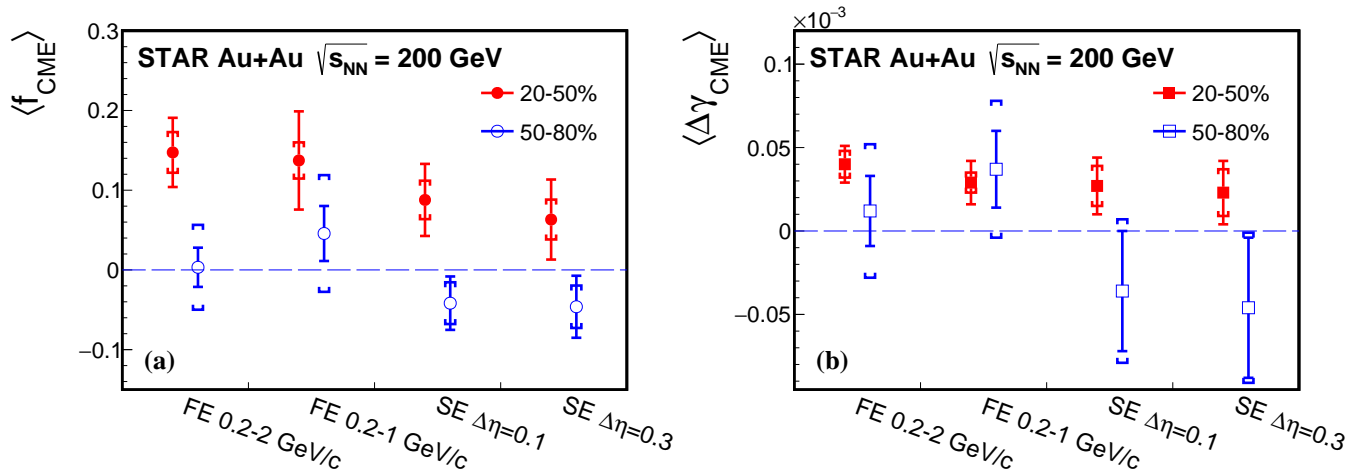


FIG. 3. The flow-background removed $\langle f_{\text{CME}} \rangle$ (a) and $\langle \Delta\gamma_{\text{CME}} \rangle$ (b) signal in 50–80% (open markers) and 20–50% (solid markers) centrality Au+Au collisions at $\sqrt{s_{\text{NN}}} = 200$ GeV, extracted by various analysis methods (FE: full-event, SE: sub-event) and kinematic cuts. Error bars show statistical uncertainties; the caps indicate the systematic uncertainties.

η gaps between the sub-events. The inclusive $\Delta\gamma$ measurements with respect to ψ_{ZDC} and ψ_{TPC} are found to be largely dominated by backgrounds, consistent with conclusions from previous measurements. Because ψ_{ZDC} aligns better with the spectator proton plane and ψ_{TPC} aligns better with the v_2 harmonic plane, these measurements can be used to extract the possible residual CME signals, assuming that the background is proportional to v_2 and the magnetic field is determined by the spectator protons. Under these assumptions, the possible residual CME signals are extracted using the new method in this paper. Some indication of finite signals is seen with a significance of 1–3 standard deviations from the sub-event to full-event methods. However, significant non-flow effects (especially for the full-event method without η gap) may still be present that warrant further investigation.

Acknowledgments. We thank the RHIC Operations Group and RCF at BNL, the NERSC Center at LBNL, and the Open Science Grid consortium for providing resources and support. This work was supported in part by the Office of Nuclear Physics within the U.S. DOE Office of Science, the U.S. National Science Foundation, the

Ministry of Education and Science of the Russian Federation, National Natural Science Foundation of China, Chinese Academy of Science, the Ministry of Science and Technology of China and the Chinese Ministry of Education, the Higher Education Sprout Project by Ministry of Education at NCKU, the National Research Foundation of Korea, Czech Science Foundation and Ministry of Education, Youth and Sports of the Czech Republic, Hungarian National Research, Development and Innovation Office, New National Excellency Programme of the Hungarian Ministry of Human Capacities, Department of Atomic Energy and Department of Science and Technology of the Government of India, the National Science Centre of Poland, the Ministry of Science, Education and Sports of the Republic of Croatia, RosAtom of Russia and German Bundesministerium für Bildung, Wissenschaft, Forschung und Technologie (BMBF), Helmholtz Association, Ministry of Education, Culture, Sports, Science, and Technology (MEXT) and Japan Society for the Promotion of Science (JSPS).

* Deceased

- [1] T. D. Lee and G. C. Wick, Phys. Rev. **D9**, 2291 (1974).
- [2] D. Kharzeev, R. D. Pisarski, and M. H. G. Tytgat, Phys. Rev. Lett. **81**, 512 (1998).
- [3] D. Kharzeev and R. D. Pisarski, Phys. Rev. **D61**, 111901 (2000).
- [4] D. E. Kharzeev, L. D. McLerran, and H. J. Warringa, Nucl. Phys. **A803**, 227 (2008).
- [5] K. Fukushima, D. E. Kharzeev, and H. J. Warringa, Phys. Rev. **D78**, 074033 (2008).
- [6] M. Asakawa, A. Majumder, and B. Muller, Phys. Rev. **C81**, 064912 (2010).
- [7] A. Bzdak and V. Skokov, Phys. Lett. **B710**, 171 (2012).
- [8] B. Muller and A. Schafer, Phys. Rev. **C82**, 057902 (2010).
- [9] D. E. Kharzeev, Prog. Part. Nucl. Phys. **75**, 133 (2014).
- [10] D. E. Kharzeev, J. Liao, S. A. Voloshin, and G. Wang, Prog. Part. Nucl. Phys. **88**, 1 (2016).
- [11] X.-G. Huang, Rept. Prog. Phys. **79**, 076302 (2016).
- [12] D. Kharzeev and J. Liao, Nat. Rev. Phys. **3**, 55 (2021).
- [13] J. Zhao, Int. J. Mod. Phys. **A33**, no.13, 1830010 (2018).
- [14] J. Zhao, Z. Tu, and F. Wang, Nucl. Phys. Rev. **35**, 225 (2018).
- [15] J. Zhao and F. Wang, Prog. Part. Nucl. Phys. **107**, 200 (2019).
- [16] W. Li and G. Wang, Annu. Rev. Nucl. Part. Sci. **70**, 293 (2020).
- [17] S. A. Voloshin, Phys. Rev. Lett. **105**, 172301 (2010).
- [18] V. Koch, S. Schlichting, V. Skokov, P. Sorensen, J. Thomas, S. Voloshin, G. Wang, and H.-U. Yee, Chin. Phys. **C41**, 072001 (2017).
- [19] H. Xu, J. Zhao, X. Wang, H. Li, Z. Lin, C. Shen, and F. Wang, Chin. Phys. C **42**, 084103 (2018).
- [20] B. Alver *et al.* (PHOBOS), Phys. Rev. Lett. **98**, 242302 (2007).
- [21] B. Alver *et al.*, Phys. Rev. **C77**, 014906 (2008).
- [22] H. Xu, X. Wang, H. Li, J. Zhao, Z. Lin, C. Shen, and F. Wang, Phys. Rev. Lett. **121**, 022301 (2018).
- [23] S. A. Voloshin, Phys. Rev. **C70**, 057901 (2004).
- [24] J.-Y. Ollitrault, Phys. Rev. **D46**, 229 (1992).
- [25] B. I. Abelev *et al.* (STAR), Phys. Rev. **C81**, 054908 (2010).
- [26] B. I. Abelev *et al.* (STAR), Phys. Rev. Lett. **103**, 251601 (2009).
- [27] L. Adamczyk *et al.* (STAR), Phys. Rev. **C88**, 064911 (2013).
- [28] L. Adamczyk *et al.* (STAR), Phys. Rev. Lett. **113**, 052302 (2014).
- [29] B. Abelev *et al.* (ALICE), Phys. Rev. Lett. **110**, 012301 (2013).
- [30] F. Wang, Phys. Rev. **C81**, 064902 (2010).
- [31] A. Bzdak, V. Koch, and J. Liao, Phys. Rev. **C81**, 031901 (2010).
- [32] S. Schlichting and S. Pratt, Phys. Rev. **C83**, 014913 (2011).
- [33] L. Adamczyk *et al.* (STAR), Phys. Rev. **C89**, 044908 (2014).
- [34] F. Wang and J. Zhao, Phys. Rev. **C95**, 051901 (R) (2017).
- [35] A. M. Poskanzer and S. Voloshin, Phys. Rev. **C58**, 1671 (1998).
- [36] V. Khachatryan *et al.* (CMS), Phys. Rev. Lett. **118**, 122301 (2017).
- [37] A. M. Sirunyan *et al.* (CMS collaboration), Phys. Rev. C **97**, 044912 (2018).
- [38] J. Adam *et al.* (STAR), Phys. Lett. **B798**, 134975 (2019).
- [39] R. Belmont and J. L. Nagle, Phys. Rev. **C96**, 024901 (2017).
- [40] J. Adam *et al.* (STAR), (2020), arXiv:2006.05035 [nucl-ex].
- [41] J. Adam *et al.* (STAR), (2020), arXiv:2006.04251 [nucl-ex].
- [42] S. Acharya *et al.* (ALICE), Phys. Lett. **B777**, 151 (2018).
- [43] S. A. Voloshin, Phys. Rev. C **98**, 054911 (2018).
- [44] P. Bozek, W. Broniowski, and J. Moreira, Phys. Rev. C **83**, 034911 (2011).
- [45] K. Xiao, F. Liu, and F. Wang, Phys. Rev. C **87**, 011901 (2013).
- [46] J. Jia and P. Huo, Phys. Rev. C **90**, 034905 (2014).
- [47] S. Shi, Y. Jiang, E. Lilleskov, and J. Liao, Annals Phys. **394**, 50 (2018).
- [48] C. Adler, A. Denisov, E. Garcia, M. J. Murray, H. Strobele, and S. N. White, Nucl. Instrum. Meth. **A470**, 488 (2001).
- [49] J. Adams *et al.* (STAR), Phys. Rev. C **73**, 034903 (2006).
- [50] K. H. Ackermann *et al.* (STAR), Nucl. Instrum. Meth. **A499**, 624 (2003).
- [51] M. Anderson *et al.*, Nucl. Instrum. Meth. **A499**, 659 (2003).
- [52] K. H. Ackermann *et al.* (STAR), Nucl. Phys. **A661**, 681 (1999).
- [53] G. Contin *et al.*, Nucl. Instrum. Meth. A **907**, 60 (2018).
- [54] B. I. Abelev *et al.* (STAR), Phys. Rev. C **79**, 034909 (2009).
- [55] H. Petersen, T. Renk, and S. A. Bass, Phys. Rev. **C83**, 014916 (2011).
- [56] J. Zhao, Y. Feng, H. Li, and F. Wang, Phys. Rev. C **101**, 034912 (2020).
- [57] R. Barlow, arXiv:hep-ex/0207026.
- [58] J. Zhao, H. Li, and F. Wang, Eur. Phys. J. C **79**, 168 (2019).